High Bandwidth Sensorless Algorithm for AC Machines Based on Square-wave Type Voltage Injection

Young-doo Yoon
Student Member, IEEE
Seoul National University
Seoul, Korea
birdy003@eepel.snu.ac.kr

Seung-ki Sul
Fellow, IEEE
Seoul National University
Seoul, Korea
sulsk@plaza.snu.ac.kr

Shinya Morimoto
Yaskawa Electric Co.
Kitakyushu 803-8530, Japan
sinya@yaskawa.co.jp

Kozo Ide
Member, IEEE
Yaskawa Electric Co.
Kitakyushu 803-8530, Japan
kozo@yaskawa.co.jp

Abstract -- **This paper describes a new control algorithm which can enhance the dynamics of a sensorless control system and gives a precise sensorless control performance. When high frequency injection methods with conventional manners (sinusoidal voltage injection) are used, Low Pass Filters (LPFs) should be used to get an error signal. However, these LPFs degrade sensorless control performances due to the time delay of LPFs themselves. To avoid this effect, the proposed method uses square wave type voltage injection instead of the sinusoidal type voltage injection. As the result, the error signal can be calculated without any delay, and the position estimation performance can be enhanced. This paper contains the voltage injection method and corresponding signal processing method. Using the proposed method, the performance of sensorless control can be enhanced remarkably. The bandwidth of current controller was enhanced up to 250 Hz and that of speed controller was up to 50 Hz.**

Index Terms—**AC machines, induction machine, sensorless control, signal injection, synchronous machine, square-wave voltage**

INTRODUCTION

Sensorless drives of AC motors are adopted in many applications which are being widespread from industrial applications to electric household appliances. Recently, electric vehicle applications are also reported [1]-[3]. The advantages of sensorless drives are not only the reduction in the cost and size but also the improvement of the reliability by eliminating the position sensor and related cable connections. To achieve the advantages, many sensorless techniques for estimating rotor position and speed have been reported. These techniques are classified into two categories: techniques based on back-EMF [4]-[7] and techniques based on saliency in spatial impedance of the motor [8]-[16].

The former uses voltage models [4], [5] and/or observers [6], [7] in the synchronous or stationary frame. It presents good results in the middle and high speed regions. Since the amplitude of back EMF is proportional to the rotor speed, it cannot keep the performance in the low speed region including zero speed and/or frequency where the back EMF disappears. The latter are exploiting the magnetic saliency. Some algorithms inject test voltage signals in a sampling period to estimate rotor position [8], [9]. Since they detect inductance difference using voltage signals in a short time, they can be frail to parameter variation or measurement noises. Other algorithms inject rotating high frequency voltages and uses tracking algorithm [10], [11]. The other algorithms inject fluctuating high frequency voltages [12]-[16]. These rotating and fluctuating high frequency voltage injection methods were proposed for zero and/or low frequency operation. These methods can be applied to general AC machines. It gives reasonable torque control capability at zero and/or low frequency, even under heavily loaded condition.

Based on such progresses, sensorless algorithms are adopted in many applications. However, the performance of the conventional sensorless control methods is still insufficient in some of application field. The bandwidth of speed controller is limited up to a few Hz.

In this paper, a new algorithm of sensorless control for AC servo applications is proposed to enhance the performance of sensorless drive remarkably. Considering zero and low speed operations, this study focused on the only voltage injection method. The method based on back-emf voltage is not considered. Therefore, the proposed sensorless algorithm injects high frequency voltage up to rated speed. However, the proposed method can be combined with the method based on back-emf voltage in middle and high speed operations just like other previous methods [1], [16].

When high frequency injection methods with conventional manners (sinusoidal voltage injection) are used, Low Pass Filters (LPFs) should be used to get an error signal. However, these LPFs degrade sensorless control performances severely because of the inherent time delay of LPFs. To enhance the performance, the delay should be minimized or removed. The proposed method relies on higher frequency square-wave type voltage injection. As a result, the error signal can be calculated without any LPF, and that means no time delay. Hence, the position estimation performance can be enhanced remarkably. As a consequence, bandwidths of current, speed and position controllers can be increased very much compared to those by the conventional sinusoidal type voltage injection method.

ANALYSIS OF CONVENTIONAL SENSORLESS ALGORITHM

Conventional sensorless algorithms [10]-[16] based on high frequency injection method exploit saliency of the motor at the injected high frequency. Using this saliency with a high

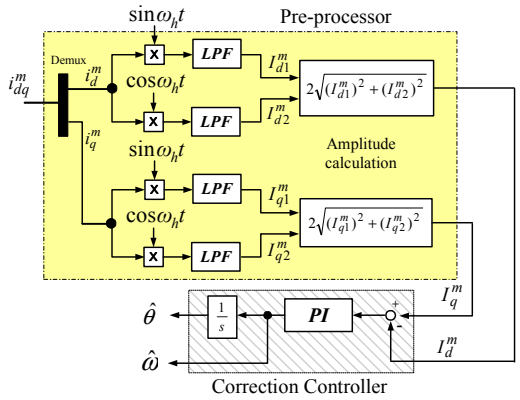

Fig. 1 Block diagram of a signal processing and a position observer

frequency injection method, sensorless algorithms extract the angle information. This process is called as a signal processing. And then, a position observer estimates rotor position. Fig. 1 shows a typical block diagram of signal processing methods including a correction controller. In this section, conventional voltage injection method and signal processing method are explained. Challenges to increase the bandwidth of the sensorless control are also addressed.

Analysis of Voltage Injection Method

In Fig. 2, the block diagram of conventional high frequency voltage injection method is shown [10]-[16]. High frequency voltage in the rotor reference frame is added to the output of the current controller. Though, in the block diagram, the high frequency voltage is injected in the rotor reference frame, the voltage can be injected in the stationary reference frame, too.

There are roughly two kinds of voltage injection methods. One is a rotating voltage injection method in the stationary reference frame [10], [11]. The other is a fluctuating voltage injection method in d-axis of the estimated rotor reference frame [12]-[16].

Basic information of every signal processing method is the induced high frequency current in the stationary reference frame, i^s_{dqsh}, which is the only measurable quantity [12]. So, i^s_{dqsh} should be analyzed according to voltage injection methods. In here, a fluctuating voltage injection method in d-axis of the estimated rotor reference frame will be analyzed.

When a fluctuating voltage is injected in d-axis of the estimated rotor reference frame, injected high frequency voltage can be described as (1) with the assumption of that the estimation error of rotor position ($\tilde{\theta}_r = \theta_r - \hat{\theta}_r$) is small enough.

$$V^{\hat{r}}_{ds} = \cos\omega t\,,\quad V^{\hat{r}}_{qs} = 0\,,\quad \tilde{\theta}_r = \theta_r - \hat{\theta}_r \approx 0\,. \tag{1}$$

The relationship between the induced high frequency current and voltage can be described as follows.

$$\begin{bmatrix} v^r_{dsh} \\ v^r_{qsh} \end{bmatrix} = [Z^r]\begin{bmatrix} i^r_{dsh} \\ i^r_{qsh} \end{bmatrix} = [Z^r][R(\theta_r)]\begin{bmatrix} i^s_{dsh} \\ i^s_{qsh} \end{bmatrix}. \tag{2}$$

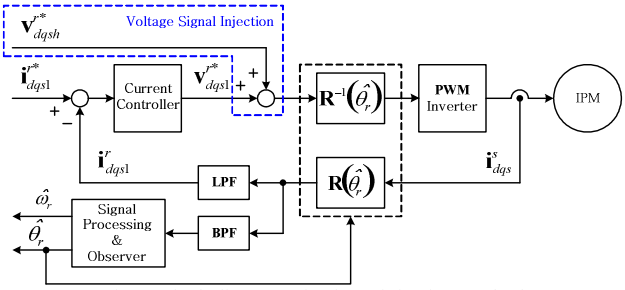

Fig. 2 Block diagram of voltage injection method

Therefore, the induced high frequency current can be described as follows.

$$\begin{bmatrix} i^s_{dsh} \\ i^s_{qsh} \end{bmatrix} = [R(\theta_r)]^{-1}[Z^r]^{-1}\begin{bmatrix} v^r_{dsh} \\ v^r_{qsh} \end{bmatrix} = [R(\theta_r)]^{-1}[Z^r]^{-1}[R(\tilde{\theta}_r)]\begin{bmatrix} v^{\hat{r}}_{dsh} \\ v^{\hat{r}}_{qsh} \end{bmatrix}. \tag{3}$$

$\omega_h L^r_{dh}$ and $\omega_h L^r_{qh}$ are generally much larger than R^r_{dh} and R^r_{qh} in the high frequency impedance model. And, the injected frequency, ω_h, is also at least one order larger than the fundamental frequency, ω_r. Therefore, high frequency impedance in the rotor reference frame, Z^r, can be simplified as follows.

$$[Z^r] = \begin{bmatrix} R^r_{dh} + L^r_{dh}\cdot s & -\omega_r L^r_{qh} \\ \omega_r L^r_{dh} & R^r_{qh} + L^r_{qh}\cdot s \end{bmatrix} \approx \begin{bmatrix} L^r_{dh}\cdot s & 0 \\ 0 & L^r_{qh}\cdot s \end{bmatrix}. \tag{4}$$

Using (3) and (4), the induced high frequency current can be represented as follows.

$$\begin{bmatrix} i^s_{dsh} \\ i^s_{qsh} \end{bmatrix} \approx \frac{\sin\omega_h t}{\omega_h}\begin{bmatrix} \dfrac{\cos(\theta_r)\cos(\tilde{\theta}_r)}{L^r_{dh}} + \dfrac{\sin(\theta_r)\sin(\tilde{\theta}_r)}{L^r_{qh}} \\ \dfrac{\sin(\theta_r)\cos(\tilde{\theta}_r)}{L^r_{dh}} - \dfrac{\cos(\theta_r)\sin(\tilde{\theta}_r)}{L^r_{qh}} \end{bmatrix} \tag{5}$$

$$\approx \frac{\sin\omega_h t}{\omega_h L^r_{dh}}\begin{bmatrix} \cos(\theta_r) \\ \sin(\theta_r) \end{bmatrix}. \left(\text{Under the assumption that } \tilde{\theta}_r \approx 0\right)$$

When rotor position, θ_r, changes from $-\pi$ to π as shown in Fig. 3, the induced high frequency current, i^s_{dqsh}, is appeared as shown in Fig. 4 which is the simulation results using the aforementioned sensorless control. Here, the envelope of the d-axis induced high frequency current shows the cosine function of rotor position and that of the q-axis induced high frequency current shows the sine function of rotor position.

To demonstrate this definitely, the bold lines are also displayed in Fig. 4 together with the d-axis and q-axis induced high frequency currents. The bold line in d-axis waveform shows $\cos(\theta_r)$ and that in q-axis waveform shows $\sin(\theta_r)$. From this figure, it can be concluded that it is possible to detect rotor position by tracking the envelope of the induced high frequency current, i^s_{dqsh}, when a high frequency voltage is injected in d-axis of the estimated rotor reference frame under the assumption of small enough error

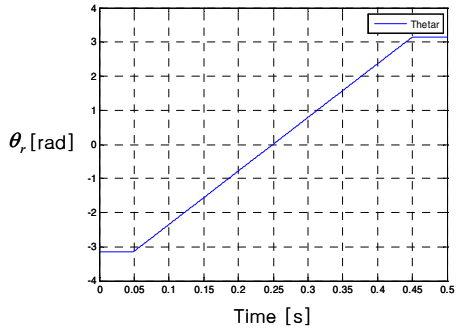

Fig. 3 Variation of the rotor angle to verify the characteristics of the induced high frequency current

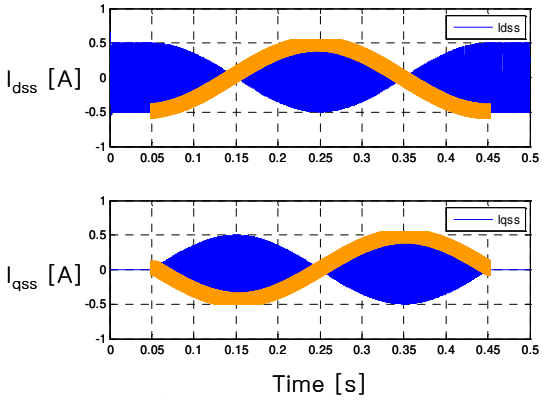

Fig. 4 Envelope of the induced high frequency current

between the actual rotor position and the estimated position.

Therefore the rotor position can be extracted only by rejecting the injected frequency from the induced high frequency current, i^s_{dqsh} as following equation. Using arctangent function as (6), rotor position can be directly calculated. In real system, however, to implement (6) is quite difficult since the denominator of (6) could be very small and/or zero in every cycle of the injected signal and the angle through (6) is sensitive to the measurement noises.

$$\frac{1}{\sin\omega_h t}\begin{bmatrix} i^s_{dsh} \\ i^s_{qsh} \end{bmatrix} \approx \frac{1}{L^r_{dh}\omega_h}\begin{bmatrix} \cos(\theta_r) \\ \sin(\theta_r) \end{bmatrix} \quad (\because \ \tilde{\theta}_r \approx 0),$$

$$\theta_{rCal} = \text{atan2}\left(i^s_{qsh} / \sin\omega_h t \, , \, i^s_{dsh} / \sin\omega_h t \right) \tag{6}$$

Signal Processing Method

When a fluctuating voltage injection method in d-axis of the estimated rotor reference frame is applied, two kinds of signal methods can be generally utilized. Theses methods can be classified by a current measurement reference frame. One is Dr. Ha's method [12], [13] which uses the current at the reference frame offset by 45° from the estimated rotor reference frame. The other could be called as "Method using $i^{\hat{r}}_{qsh}$" [14], [15] which uses q-axis current in the estimated rotor reference frame. Here, the method in [15] will be analyzed.

Fig. 5 shows the block diagram of "Method using $i^{\hat{r}}_{qsh}$."

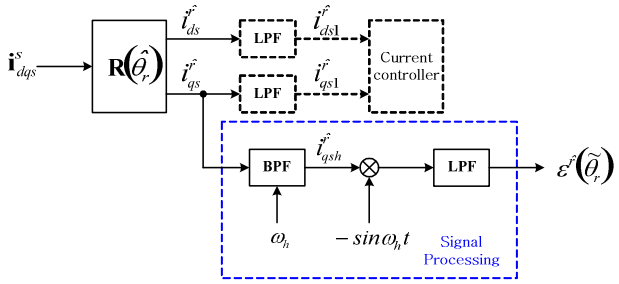

Fig. 5 Block diagram of "Method using $i^{\hat{r}}_{qsh}$"

As shown in Fig. 5, this method uses q-axis induced high frequency current in the estimated rotor reference frame. The main idea for this method is that the injected voltage at d-axis in the real rotor reference frame should induce only d-axis current.

The high frequency model of the plant can be described as

$$\begin{bmatrix} v^r_{dsh} \\ v^r_{qsh} \end{bmatrix} = \begin{bmatrix} R^r_{dh} + L^r_{dh}\cdot s & -\omega_r L^r_{qh} \\ \omega_r L^r_{dh} & R^r_{qh} + L^r_{qh}\cdot s \end{bmatrix}\begin{bmatrix} i^r_{dsh} \\ i^r_{qsh} \end{bmatrix}. \tag{7}$$

From (7), $-i^{\hat{r}}_{qsh}\sin\omega_h t$ can be described as follows.

$$-i^{\hat{r}}_{qsh}\sin\omega_h t = \frac{V_{inj}}{2}\left[\frac{\omega_r L^r_{diff} - 2\omega_r L^r_{avg}\cos 2\tilde{\theta}_r}{2\omega_h^2 L^r_{dh} L^r_{qh}}\sin 2\omega_h t + \frac{L^r_{diff}\sin 2\tilde{\theta}_r}{\omega_h L^r_{dh} L^r_{qh}}\frac{1+\cos 2\omega_h t}{2} \right]. \tag{8}$$

$$L^r_{avg} \equiv \frac{L^r_{dh} + L^r_{qh}}{2}, \quad L^r_{diff} \equiv L^r_{dh} - L^r_{qh}. \tag{9}$$

As shown in (8), estimation error of rotor position, $\tilde{\theta}_r \equiv \theta_r - \hat{\theta}_r$, is included. Error signals including $\tilde{\theta}_r$ can be extracted by using a low pass filter. Equation (10) shows the result after ideal low pass filtering.

$$LPF\left(-i^{\hat{r}}_{qsh}\sin\omega_h t\right) = \frac{V_{inj} L^r_{diff}}{4\omega_h L^r_{dh} L^r_{qh}}\sin 2\tilde{\theta}_r \equiv \varepsilon^{\hat{r}}\left(\tilde{\theta}_r\right). \tag{10}$$

Though only one signal processing method has been addressed here, all signal processing methods with high frequency injection have something in common. All of them use LPFs to get error signals. Using LPF is inevitable since the injected frequency component should be rejected by LPF. However, LPF results in a time delay in position and speed estimation and this delay limits all the performance of sensorless control.

Challenges to Increase Bandwidth of Sensorless Control

Conventional position observer-correction controller- may be the form of a PI controller or a form of a PID controller with torque feed-forward. As mentioned in the previous section, signal processing methods incorporate LPF to obtain an estimation error of rotor position. Furthermore, the speed estimation, used as feedback signal for the speed control loop, also needs LPF since the estimated speed from the position observer is noisy. Therefore, the realistic implementation of a position observer is not a simple form of

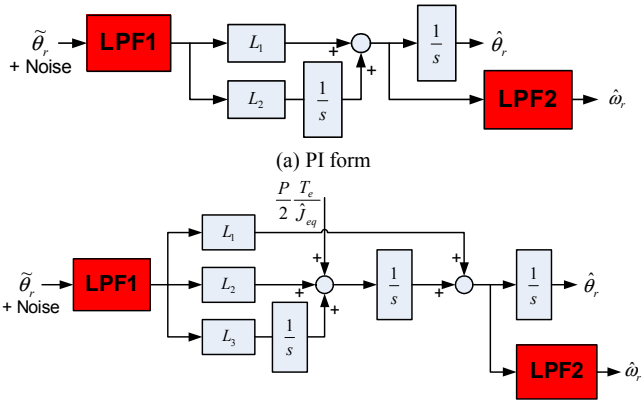

(a) PI form

(b) PID form

Fig. 6 Realistic forms of conventional position observer

a PI or PID controller. Fig. 6 shows a possible implementation of position and speed observer. As shown in Fig. 6, LPF1 and LPF2 are included in the position observer loop.

These LPFs restrict the control bandwidth. At first, LPF1 is related with the bandwidth of the position observer. When the cut off frequency of LPF1 is high, that means that LPF1 is weak, the input of the position observer has severe noise. And, when LPF1 is strong, that means that the cut off frequency of LPF1 is low, the position observer loop has severe time delay. Therefore, in both cases, the bandwidth of the position observer is restricted. Because of the noise sensitivity and the delay, it makes the observer unstable when the bandwidth is tempted to increase.

LPF2 is related with the bandwidth of the speed controller. When LPF2 is weak, the feedback of the speed controller has severe noise. And, when LPF2 is strong, it makes severe delay in speed controller loop. In both case, the bandwidth of the speed controller is also restricted. Because of the noise sensitivity and the delay, it degrades the performance of the speed controller when the bandwidth is getting extended.

Until now, the realistic implementation of the position observer is analyzed. As mentioned before, LPFs restrict the bandwidth of position observer and speed controller. Therefore, in order to increase bandwidths, LPFs should be eliminated or be weak. And, the input of position observer should have vitually no noise to eliminate the LPFs. Practically those are impossible to achieve.

PROPOSED SENSORLESS ALGORITHM

Square-wave Type Voltage Injection Method

As mentioned before, the envelope of i^s_{dqsh} (bold lines) in Fig. 4 means the rotor position. Therefore, rotor position can be extracted only by rejecting the injected high frequency from the induced current, i^s_{dqsh}. Using arctangent function as (6), rotor position can be directly calculated. In this case, LPF may not be used to get rotor position and there is no delay in rotor position estimation. In real system, however, (6) is not possible to be implemented as described before.

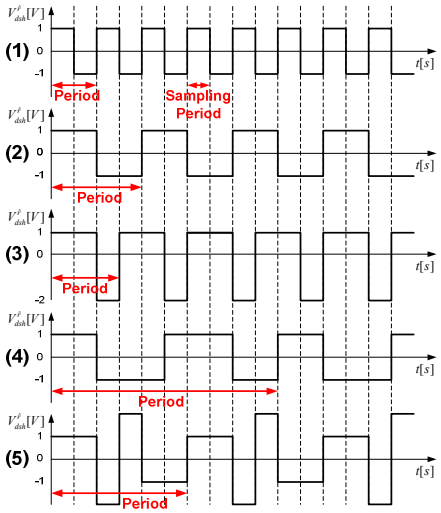

Fig. 7 Several possible square-wave type injection voltages

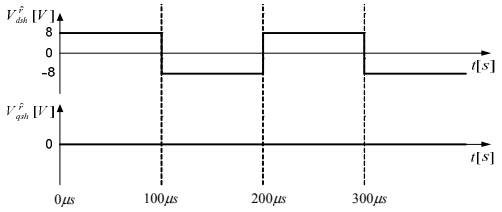

Fig. 8 Pattern of a square-wave type injection voltage described by (11)

In order to get a rotor position as (6) in real system, the high frequency sine function, $\sin \omega_h t$, should be eliminated from i^s_{dqsh}. To that purpose, a method to inject square-wave type voltage in d-axis of the estimated rotor reference frame can be used. The injected voltage is described as

$$V^{\hat{r}}_{dsh} = \begin{cases} V_h, & half\ duty \\ -V_h, & otherwise \end{cases} \quad (V_h > 0),\ V^{\hat{r}}_{qsh} = 0 \qquad (11)$$

where V_h is the magnitude of injection voltage. The injected voltage can be several different square-wave type voltages as shown in Fig. 7. However, for convenience of the explanation, the voltage described by (11), shown in Fig. 7 (2), is used for the analysis.

To get better performances, the maximum injection frequency can be up to a half of the switching frequency. The reason is for the digital implementation of notch filter which is used for the feedback of current controller. If the high frequency induced current is not properly filtered and the filtered current is utilized for the feedback of the current regulator, the output voltage of the current regulator would be interfered with the high frequency injection voltage and it would degrade the performance. Another reason is to prevent the induced current from the noise current due to the sampling delay and/or the component in the switching frequency. Furthermore, if the space vector PWM modulation is used to apply voltage into the motor, the noise current would be minimized due to the symmetric voltage pulse pattern.

Fig. 8 shows the pattern of injection voltage under the condition of that the switching frequency is 10 kHz and injection frequency is 5 kHz and the magnitude of injection voltage is 8 V. These values depend on motor plants and the desired performance.

When the square-wave type voltage in Fig. 8 is injected, corresponding Δi^s_{dqsh} can be described as (12).

$$\begin{bmatrix}\Delta i^s_{dsh}\\ \Delta i^s_{qsh}\end{bmatrix} = [R(\theta_r)]^{-1}[Z^r]^{-1}\left[R(\tilde{\theta}_r)\right]\begin{bmatrix}v^{\hat{r}}_{dsh}\\ v^{\hat{r}}_{qsh}\end{bmatrix}$$

$$\approx \begin{cases} V_h\Delta T\cdot\begin{bmatrix}\dfrac{\cos(\theta_r)\cos(\tilde{\theta}_r)}{L^r_{dh}}+\dfrac{\sin(\theta_r)\sin(\tilde{\theta}_r)}{L^r_{qh}}\\ \dfrac{\sin(\theta_r)\cos(\tilde{\theta}_r)}{L^r_{dh}}-\dfrac{\cos(\theta_r)\sin(\tilde{\theta}_r)}{L^r_{qh}}\end{bmatrix}, V^{\hat{r}}_{dsh}>0 \\ -V_h\Delta T\cdot\begin{bmatrix}\dfrac{\cos(\theta_r)\cos(\tilde{\theta}_r)}{L^r_{dh}}+\dfrac{\sin(\theta_r)\sin(\tilde{\theta}_r)}{L^r_{qh}}\\ \dfrac{\sin(\theta_r)\cos(\tilde{\theta}_r)}{L^r_{dh}}-\dfrac{\cos(\theta_r)\sin(\tilde{\theta}_r)}{L^r_{qh}}\end{bmatrix}, V^{\hat{r}}_{dsh}<0 \end{cases} \quad (12)$$

To consider the polarity of the injection voltage, (12) can be modified as (13).

$$\Delta i^{s\,\prime}_{dsh} = \begin{cases}\Delta i^s_{dsh}, \textit{if } V^{\hat{r}}_{dsh}>0\\ -\Delta i^s_{dsh}, \textit{otherwise}\end{cases}, \Delta i^{s\,\prime}_{qsh} = \begin{cases}\Delta i^s_{qsh}, \textit{if } V^{\hat{r}}_{dsh}>0\\ -\Delta i^s_{qsh}, \textit{otherwise}\end{cases} \quad (13)$$

Finally, $\Delta i^{s\,\prime}_{dqsh}$ can be expressed as (14)

$$\begin{bmatrix}\Delta i^{s\,\prime}_{dsh}\\ \Delta i^s_{qsh}\end{bmatrix} = V_h\Delta T\cdot\begin{bmatrix}\dfrac{\cos(\theta_r)\cos(\tilde{\theta}_r)}{L^r_{dh}}+\dfrac{\sin(\theta_r)\sin(\tilde{\theta}_r)}{L^r_{qh}}\\ \dfrac{\sin(\theta_r)\cos(\tilde{\theta}_r)}{L^r_{dh}}-\dfrac{\cos(\theta_r)\sin(\tilde{\theta}_r)}{L^r_{qh}}\end{bmatrix} \quad (14)$$

$$\approx \frac{V_h\Delta T}{L^r_{dh}}\cdot\begin{bmatrix}\cos(\theta_r)\\ \sin(\theta_r)\end{bmatrix} \text{ (Under assumption that } \tilde{\theta}_r\approx 0).$$

Using $\Delta i^{s\,\prime}_{dqsh}$, the calculated rotor position, θ_{rCal}, can be directly calculated as (15). And, the error signal of the position observer, $f(\tilde{\theta}_r)$, can be also directly calculated from θ_{rCal} as (16). Therefore, θ_{rCal} and $f(\tilde{\theta}_r)$ can be obtained at every sampling instant without any LPF and there is no time delay.

$$\theta_{rCal} = \text{atan2}\left(\Delta i^{s\,\prime}_{qsh}, \Delta i^{s\,\prime}_{dsh}\right) \quad (15)$$

$$f_1(\tilde{\theta}_r) \equiv \theta_{rCal} - \hat{\theta}_r \approx K_{error1}\tilde{\theta}_r \qquad \left(\tilde{\theta}_r \approx 0\right) \quad (16)$$

Using the proposed method, the error signal of the position observer, $f(\tilde{\theta}_r)$, can be obtained with no LPF. Therefore, LPF1 shown in Fig. 6 can be eliminated. To further remove LPF2, the speed controller can be implemented based on another state of the position observer for a feedback. Fig. 9 shows the final block diagram of the position observer exploiting the advantage of the proposed method.

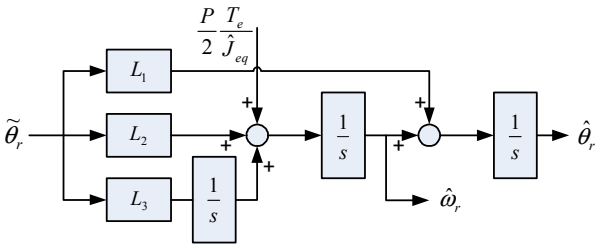

Fig. 9 Block diagram of the proposed position observer

TABLE I
NOMINAL PARAMETER OF THE TESTED MOTOR

Quantity	Value [Unit]
Rated Power	80 [W]
Rated Torque	0.5 [Nm]
Rated Current	2.1 [A_{RMS}]
Rated Speed	1500 [r/min]
Dc Link Voltage	50 [V]
Overall Inertia	11.72e-5 [kg·m^2]

Comparing Fig. 6 and Fig. 9, it can be seen that two LPFs have been disappeared in Fig. 9. It means that the major cause to limit the dynamics of sensorless control is removed. Therefore, by using the proposed method, the bandwidth of position observer and speed controller can be extended compared to that of the conventional method. The performance comparison between the conventional and the proposed signal processing method in conjunction with the new injection method and observer design can be summarized as below.

- Two low pass filters are removed.
  - ➔ Virtually no delay in tracking the rotor position
- Injection frequency becomes higher.
  - ➔ Fundamental and injection frequency are definitely separated.
- Stability of overall system is improved.
  - ➔ Bandwidth of the position observer can be increased.
  - ➔ Bandwidth of the speed and position controller can be increased.

EXPERIMENTAL RESULTS

The proposed method can be applied to any kinds of AC machines. Here, a Interior Permanent Magnet Synchronous Machine (IPMSM) was selected for experiments to verify the effectiveness of the proposed method. The nominal parameters of the tested electric machine are listed in Table. I.

Switching frequency was set as 10 kHz and sampling frequency was 20 kHz. The square wave high frequency voltage was injected. In the cases of position control and speed control, the magnitude of the injection voltage was 8 V and the frequency was 5 kHz.

The bandwidths of the speed and position controller were set as 50 Hz and 10 Hz, respectively. The pole of the position observer was set as 50 Hz and PI gains of the position observer were tuned. The bandwidth of the current controller was 250 Hz. The cut-off frequency of the notch filter for the

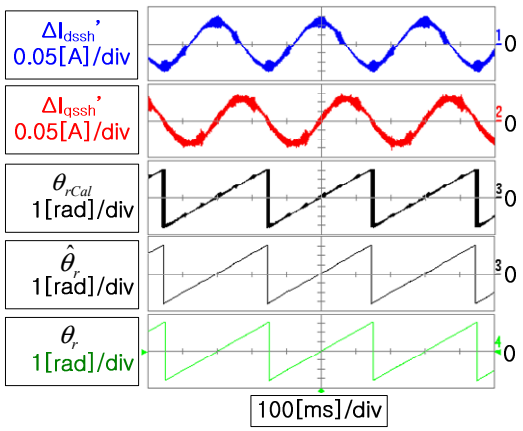

Fig. 10 Position estimation performance

feedback of current controller was set as the injection frequency.

Fig. 10 shows the position estimation performance on a constant speed operation at 100 r/min. In Fig. 10, $\Delta i^{s'}_{dqsh}$, the calculated position, θ_{rCal}, the estimated position, $\hat{\theta}_r$, and the real position, θ_r, are displayed. As shown in Fig. 10, the calculated position, θ_{rCal}, had some noises but the estimated position, $\hat{\theta}_r$ had virtually no noise due to the position observer. From this figure, it can be concluded that the proposed method estimates the rotor position quite well without any time delay.

Fig. 11 shows the current regulation performance at a stand still. D-axis current in the rotor reference frame was regulated with a sine wave reference. The magnitude of the current reference was 1 A and the frequency was 250 Hz. In Fig. 11(a) and (b), the offsets of the current reference was 0 A and 1.5 A, respectively. IdseNF represents d-axis current filtered by the notch filter. In Fig. 11(a), IdseNF was slightly distorted due to the zero current clamping effect[17]. In Fig. 11(b), IdseNF was regulated well.

Experiments on a speed control mode were performed as shown in Fig. 12, 13, and 14. Fig. 12 shows the step response when the output of the speed controller-torque reference- is not limited. The step response with the references changes from 300 r/min to 400 r/min is shown. As shown in Fig. 12, speed was well regulated and the bandwidth can be considered as the 50 Hz, which is the designed value.

Fig. 13 shows the step response when the output of the speed controller is limited. The step response with the reference change from 0 r/min to 1500 r/min is shown. As shown in Fig. 13, speed was increasing as a ramp since torque reference was saturated.

Fig. 14 shows the sine wave response of speed controller to show the bandwidth of the speed regulator clearly. The magnitude of the speed reference was set as 100 r/min and the frequencies were set as 10 Hz and 50 Hz respectively. As shown in these figures, speed was well regulated up to the designed bandwidth, which was 50Hz.

Also, the Bode plot was used for evaluating the performance of the current regulator and speed controller. Generally, the current regulation loop is considered as the 1st LPF $\left(i^{r}_{dqs}/i^{r*}_{dqs} = \omega_c/(s+\omega_c)\right)$, therefore, the bandwidth of

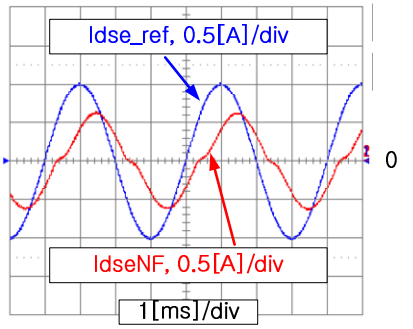

(a) The offset of current command is 0 A

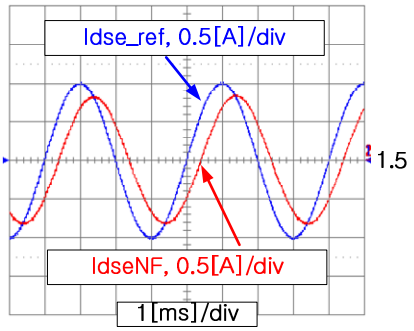

(b) The offset of current command is 1.5 A

Fig. 11 Current regulation performance

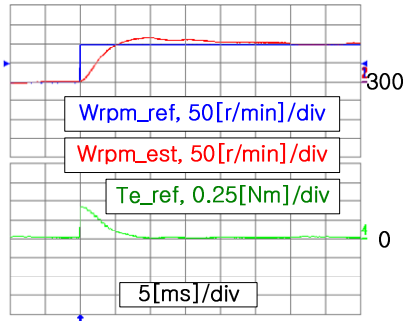

Fig. 12 Step response of speed controller when the output of the speed controller is not limited

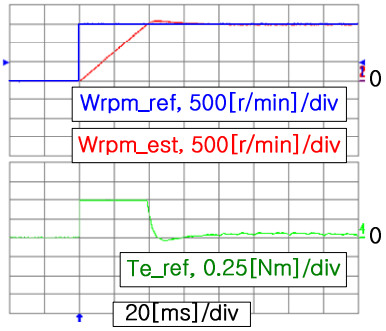

Fig. 13 Step response of speed controller when output torque is saturated

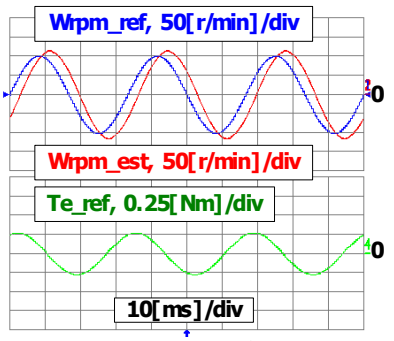

(a) 30 Hz operation

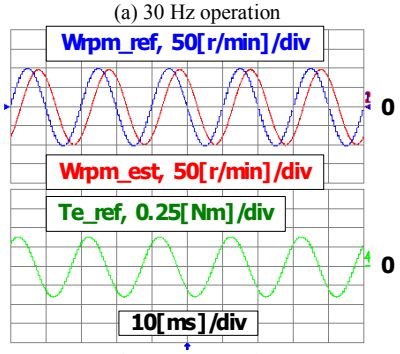

(b) 50 Hz operation

Fig. 14 Sine wave response of speed controller

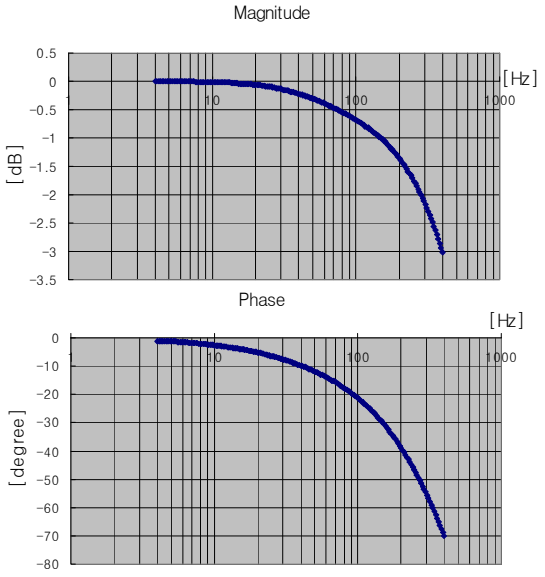

Fig. 15 Bode diagram of the current regulation performance

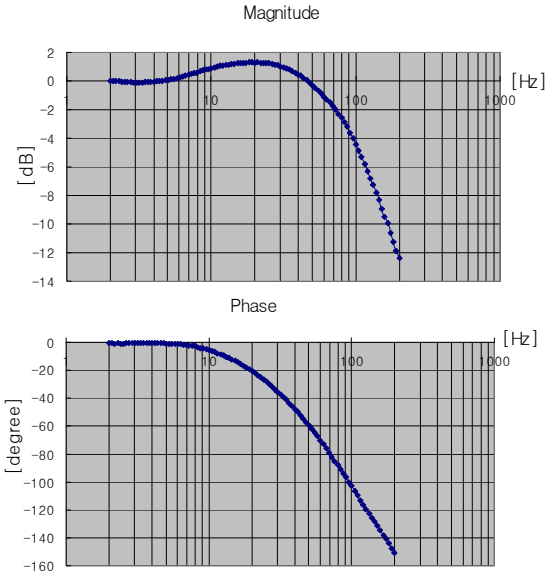

Fig. 16 Bode diagram of the speed control performance

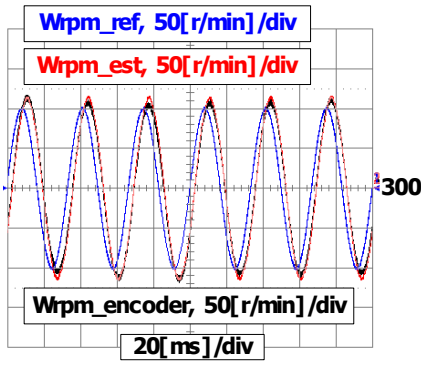

(a) 30 Hz operation

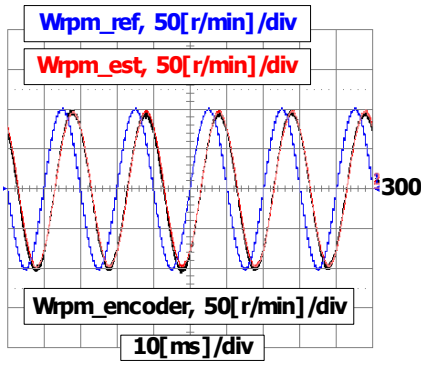

(b) 50 Hz operation

Fig. 17 Speed estimation performance of the position observer

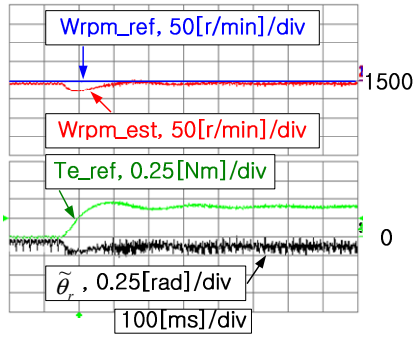

(a) From 0 % to 80 %

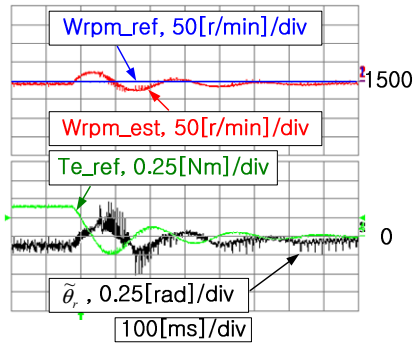

(b) From 80 % to 0 %

Fig. 18 Stiffness of the proposed sensorless algorithm with load variation

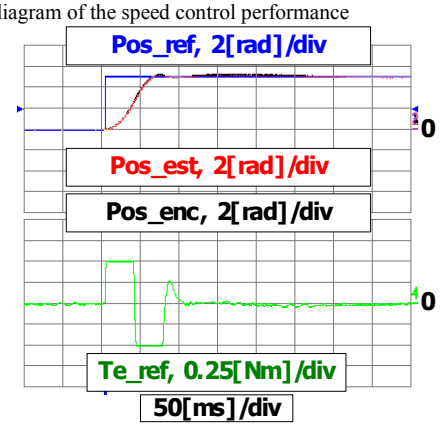

Fig. 19 Step response of the position controller

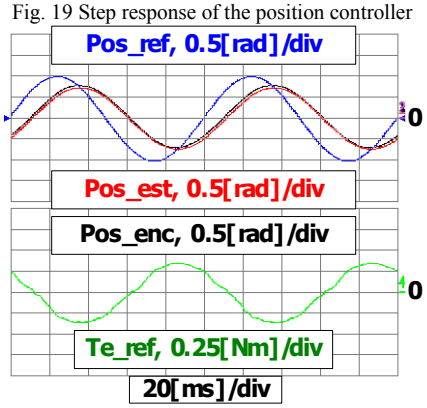

Fig. 20 Sine wave response of the position controller with reference of 10 Hz

the regulator is defined as the frequency where 3 [dB] attenuation of the actual current compared to its reference in Bode plot occurs. However, the exact transfer function of the loop including delays can not be modeled as the 1st LPF , and sometimes the frequency in Bode plot where 45 [deg] phase delay occurs may be considered as the bandwidth. Fig. 15 shows Bode plot of the current feedback loop. The bandwidth of the current regulator is almost 250 Hz.

Fig. 16 shows Bode plot of the speed feedback loop. If the frequency where 45 [deg] phase delay occurs is considered as the bandwidth of the regulator, the bandwidth of the speed regulator is almost 40 Hz. That is slightly less than the designed bandwidth.

Fig. 17 shows the speed estimation performance. The experimental condition of Fig. 17 was the same as that of Fig. 14. In these figures, speed reference (Wrpm_ref), estimated speed (Wrpm_est), and the speed from encoder (Wrpm_encoder) are displayed. 'Wrpm_encoder' is the calculated speed by M/T method [18] with an encoder. Therefore, it can be considered as a real speed. The speed reference is the signal which has the most leading phase. And other two signals are almost same as each other. As shown in these figures, the estimated speed was identical with the real speed. From these results, it can be concluded that the speed estimation by the position observer was performed well.

Fig. 18 shows the dynamic stiffness of the proposed sensorless control algorithm. On a constant speed operation of 1500 r/min, sudden load torque was applied by a load machine, DC motor. The load was varied from 0 % to 80 % and vice versa. Due to limitations of the load machine, load over 80 % could not be applied. As shown in Fig. 18, the position estimation error was maintained within ± 0.25 rad even if the load torque varied rapidly.

Experiments on position control mode were also performed. Position controller consists of only P controller. Bandwidths of the speed controller and position controller were set to 50 Hz and 10 Hz. Fig. 19 shows the step response of the position controller with the references of 0 rad to 5 rad. In the figure, position reference (Pos_ref), estimated position (Pos_est), position from encoder (Pos_enc), and torque reference (Te_ref) are displayed. 'Pos_enc' can be considered as a real position. As shown in Fig. 19, Pos_est was identical with 'Pos_enc' and position was well regulated.

Fig. 20 shows the sine wave response of position controller. Signals in Fig. 20 are same as those in Fig. 19. The magnitude of the position reference was 1 rad and the frequency was 10Hz. As shown in figure, the bandwidth of the position controller is around 10Hz, which is the designed value.

CONCLUSIONS

This paper proposes a new sensorless algorithm. It contains voltage injection method, signal processing method, and position observer. Based on the square-wave type high frequency voltage injection, a new rotor position estimation method is proposed. The estimated position has a little noise but virtually no delay.

Using the proposed method, the bandwidth of the position observer is increased up to 50 Hz. The bandwidth of the speed controller and position controller is also increased up to 50 Hz and 10 Hz, respectively. By increasing the injection frequency up to a half of the switching frequency, the fundamental frequency is definitely separated from the injection frequency. And, the bandwidth of the current controller is increased up to 250 Hz. As a result, the stability, repeatability, bandwidth, and dynamic stiffness of the proposed sensorless control method have been enhanced remarkably compared to that of a conventional method.

The feasibility and effectiveness of the proposed method have been verified through the experimental results and theoretical analysis. And it can be easily applied to any AC servo drive system driven by a PWM inverter and a digital controller.

REFERENCES

[1] M. Tursini, R. Petrella, and F. Prasiliti, "Sensorless control of an IPM synchronous motor for city-scooter application," *Conf. Rec. of IEEE IAS. Annu. Meet.*, Oct. 2003, pp. 1472-1479.

[2] R. Raute, and N. Ertugrul, "Sensorless permanent magnet AC motor drive with near zero-speed operation for electric-assisted bicycle," *in Proc. of EPE 2005-Dresden*, Sep. 2005, pp.1-10.

[3] K. Ide, M. Takaki, S. Morimoto, Y. Kawazoe, A. Maemura and M. Ohto, " Saliency-based sensorless drive of adequate designed IPM motor for robot vehicle application," *conf. rec. of PCC*, pp. 1126-1133, April 2007.

[4] S. Ogasawara and H. Akagi, "An approach to position sensorless drive for brushless dc motor," *IEEE Trans. Ind. Applicat.*, vol. 27, pp. 928–933, Sept./Oct. 1991.

[5] K. D. Hurst, T. G. Habetler, G. Griva, and F. Profumo, "Zero-speed tacholess IM torque control: simply a matter of stator voltage integration," *IEEE Trans. Ind. Applicat.*, vol. 34, pp. 790–795, July/Aug. 1998.

[6] A. B. Kulkarni and M. Ehsani, "A novel position sensor elimination technique for interior permanent-magnet synchronous drive," *IEEE Trans. Ind. Applicat.*, vol. 28, pp. 144–150, Jan./Feb. 1992.

[7] R. B. Sepe and J. H. Lang, "Real-time observer-based (adaptive) control of a permanent-magnet synchronous motor without mechanical sensors," *IEEE Trans. Ind. Applicat.*, vol. 28, pp. 1345–1352, Nov./Dec. 1992.

[8] M. Schroedl, "Sensorless control of AC machines at low speed and standstill based on the 'INFORM' method," *Conf. Rec. IEEE-IAS Annu. Meeting*, 1996, pp. 270–277.

[9] S. Ogasawara and H. Akagi, "Implementation and position control performance of a position-sensorless IPM motor drive system based on magnetic saliency," *IEEE Trans. Ind. Applicat.*, vol. 34, pp. 806–812, July/Aug. 1998.

[10] P. L. Jansen and R. D. Lorenz, "Transducerless position and velocity estimation in induction and salient AC machines," *IEEE Trans. Ind. Applicat.*, vol. 31, pp. 240–247, Mar./Apr. 1995.

[11] Y. Jeong, R.D. Lorenz, T.M. Jahns, and S. K. Sul, "Initial rotor position estimation of an interior permanent-magnet synchronous machine using carrier-frequency injection methods" *IEEE Trans. Ind. Appl.*, Vol. 41, No 1, pp. 38–45, Jan./Feb. 2005.

[12] J. I. Ha and S. K. Sul, "Sensorless field-orientation control of an induction machine by high-frequency signal injection," *IEEE Trans. Ind. Applicat.*, Jan. /Feb. 1999, vol. 35, no. 1, pp. 45-51.

[13] J. I. Ha, K. Ide, T. Sawa and S. K. Sul, "Sensorless position control and initial position estimation of an interior permanent magnet motor," *Conf. Rec. of IEEE IAS. Annual. Meeting*, Sept. 2001, vol.4 pp. 2607-2613.

[14] M. J. Corley and R. D. Lorenz, "Rotor position and velocity estimation for a permanent magnet synchronous machine at standstill and high speeds," *Conf. Rec. IEEE-IAS Annu. Meeting*, vol. 1, 1996, pp. 36–41.

[15] J. H. Jang, S. K. Sul, J. I. Ha, K. Ide, and M. Sawamura, "Sensorless drive of surface-mounted permanent-magnet motor by high-frequency signal injection based on magnetic saliency," *IEEE Trans. Ind. Applicat.*, vol. 39, pp. 1031-1039, July/Aug. 2003.

[16] K. Ide, J. K. Ha and M. Sawamura, "A hybrid speed estimation of flux observer for induction motor drives," *IEEE Trans. Ind. Electron.*, vol. 53, no. 1, February 2006.

[17] J. S. Kim, J. W. Choi and S. K. Sul, "Analysis and compensation of voltage distortion by zero current clamping in voltage-fed PWM inverter," *Conf. Rec. of IPEC-Yokohama*, 1995, pp. 265-270.

[18] T. Ohmae, T. Matsuda, K. Kamiyama and M. Tachikawa, "A microprocessor-controlled high-accuracy wide-range speed regulator for motor drives," *IEEE Trans. Ind. Electron.*, vol. 29, no. 3, August 1982.